Journal of Molecular Spectroscopy 261 (2010) 28–34

Contents lists available at ScienceDirect

Journal of Molecular Spectroscopy

journal homepage: www.elsevier.com/locate/jms

FTIR study of 11 interacting vibrational states of CH_2DI

O. Baskakov [a,*], S. Alanko [b], V.-M. Horneman [b]

[a] Department of Quantum Radiophysics, The Karazin National University, 4, Svobody Square, UA-61077 Kharkiv, Ukraine
[b] Department of Physics, P.O. BOX 3000 90014 University of Oulu, Finland

ARTICLE INFO

Article history:
Received 20 January 2010
Available online 23 February 2010

Keywords:
FTIR spectra
Methyl iodide
Vibrational state
Interaction

ABSTRACT

Rotational level structure of 12 vibrational states of CH_2DI with energies in the 1000–1800 cm^{-1} region has been retrieved from high resolution (0.001–0.003 cm^{-1}) FTIR spectra. Eleven vibrational states, namely, 2^1, $3^16^1(A')$, $5^1(A'')$, $3^16^1(A'')$, $6^2(A')$, $5^1(A')$, $6^1(A')$ $6^1(A'')$, 2^13^1, $6^2(A'')$, $3^26^1(A')$ and $3^15^1(A'')$ have been found to interact. A total of 27 919 transitions belonging to diverse fundamental, combination and hot bands were assigned and used in the combined nonlinear root mean square fit to give the band centers, rotational, centrifugal distortion and coupling parameters of the states under investigation. The RMS deviation of the fit has been demonstrated to be 0.000218 cm^{-1}. The number of the coupling parameters required to reproduce the observed spectra with the experimental uncertainty appeared to be 46.

1. Introduction

The vibration–rotation properties of methyl halides have long been a subject of great interest and the C_{3v} symmetric top varieties of methyl iodide in particular (CH_3I, $^{13}CH_3I$, CD_3I and $^{13}CD_3I$) are one of the best understood symmetric rotor molecules. They have been thoroughly investigated earlier, see e.g. [1,2], but there are relatively few high resolution infrared studies on the partially deuterated forms.

Some time ago a high resolution study of all the fundamental vibration bands of CH_2DI and CHD_2I was initiated in Oulu. To date, the lower $\nu_3(A')$ [3], $\nu_6(A')$ and $\nu_6(A'')$ [4] bands of these deuterated varieties have been analyzed. A goal of the present paper is to record and analyse FTIR spectra of the three next fundamental bands $\nu_2(A')$, $\nu_5(A')$, and $\nu_5(A'')$ of mono deuterated methyl iodide CH_2DI which are located in the energy range 1100–1500 cm^{-1}. Previously the pure rotation and vibration–rotation spectra of this asymmetric isotopologue were the subjects of several publications. Low-resolution IR spectra have been obtained by Riter and Eggers [5] (and some earlier references therein) where all nine fundamental bands have been assigned. High resolution spectra prior to works [3,4] where observed only in two studies. Das et al. reported a Doppler-limited diode laser study of part of the $\nu_6(A'')$ band [6], and Man and Butcher have recorded and analysed the $2\nu_3(A')$ and $\nu_6(A'')$ bands measured by FTIR spectrometer at a resolution of about 0.05 cm^{-1} [7]. Both these works treated the states as isolated ones. The observation of pure rotational spectra of CH_2DI in the ground vibrational state is also reported. The measurements of Mallinson [8] between 26.5 and 40 GHz permitted the determination of the three rotational constants and the five quartic centrifugal distortion constants. More recently, an international group of researchers [9] have combined microwave Fourier transform, millimeterwave and submillimeterwave spectroscopy and determined improved set of rotational and centrifugal distortion constants (up to sextic terms) together with iodine quadrupole coupling constants. In that work, to obtain more accurate results, they also used the ground state combination differences from the spectrum studied in Ref. [3].

2. Experimental details

The measurements were carried out with the BRUKER IFS 120 HR Fourier spectrometer in the Infrared laboratory at the University of Oulu. An enriched sample with the 98% purity of CH_2DI was obtained from Sigma–Aldrich Isotopes. In the present work experimental data from four measurements (A, B, C, and D in Table 1) with different optical filters and detectors were utilized. In measurement A a liquid helium (LHe) cooled bolometer was used. After adding LHe the gas above LHe in the can is evacuated down to 1867 Pa, when the bolometer is wanted to use at the temperature of 1.4–1.8 K, as we do. The used multilayer interference filters are made by Barr and Spectrogon. In the A measurement the filter was installed inside the bolometer dewar and therefore it was working at low temperature. The Si bolometer is optimized for the used spectrometer by Infrared Laboratories Inc. The liquid nitrogen cooled Mercury Cadmium Telluride (MCT) detector is made by Graseby Infrared Ltd.

In all the measurements the used optimized multi-pass sample cell [10,11] was provided with two potassium bromide (KBr) win-

* Corresponding author.
E-mail address: oibas2003@yahoo.com (O. Baskakov).

0022-2852/$ - see front matter © 2010 Elsevier Inc. All rights reserved.
doi:10.1016/j.jms.2010.02.006

Table 1
Conditions of the measurements.

	A	B	C	D
Wavenumber range (cm^{-1})	451–860	700–1040	940–1260	1230–1650
Optical filter (cm^{-1})	400–860	500–1150	850–1320	1200–1700
Detector	Si bolometer	MCT	MCT	MCT
Registration time (h)	48.1	77.8	45.3	44.5
APL (m)	3.2	3.2	9.6	3.2
Sample pressure (Pa)	52.3	64.3	10.7	64.3
Res due MOPD (cm^{-1})	0.00085	0.001	0.0012	0.0012
AB (cm^{-1})	0.00073	0.0009	0.0011	0.0015

APL, absorption path length; AB, aperture broadening; MOPD, maximum optical path difference.

dows, a glowbar source was used, and a germanium film on KBr was employed as a beam splitter. The instrumental resolution is caused together by MOPD and AB that is given in Table 1, at lower end of the wavenumber range. AB is directly proportional to the wavenumber. These instrumental effects together with the Doppler broadening gave the final spectral resolution 0.001 cm^{-1} near the lowest end of the measured spectral region, and 0.0029 cm^{-1} near the highest end. The spectra of the lowest two regions were calibrated using the ν_2 transitions of carbonyl sulfide (OCS) and the upper regions (spectrum C and D) with lines of the $2\nu_2$ band of OCS [12]. The peak positions were calculated with an optimized center of gravity method [13].

3. Details of investigation

CH_2DI is a very slightly asymmetric top having asymmetry parameter $k = -0.998$. It belongs to the point group C_s. The nine fundamental vibrations factorize into six of symmetry A', which give rise to hybrid a/b-type bands, and three of symmetry A'', which produce c-type bands. The vibrational bands under current investigation are $\nu_2(A')$, $\nu_5(A')$ and $\nu_5(A'')$ with the band centers located near 1172, 1240 and 1424 cm^{-1}, respectively [5]. On preliminary inspection, they proved to be perturbed. Obviously, the reason for this was interaction with nearby levels produced by combinations of low lying $3^1(A')$, $6^1(A')$ and $6^1(A'')$ vibrational states. All states under consideration perturb each other to a different extent. A challenging goal of the present work was to take into account, or, in other words, to include into the model, as many states and vibration–rotation interactions as would be needed to describe all the assigned transitions. Complete information on all vibrational states with energies between 1000 and 1800 cm^{-1} (with rotational levels intertwined and therefore able to interact) is given in Table 2. For the sake of convenience Table 2 contains also the energies of the lowest vibrational states.

From the very beginning we traced a chain of possible couplings between the states as follows. Previous study [4] has shown that $6^1(A')$ and $6^1(A'')$ vibrational levels located 150 cm^{-1} apart interact noticeably. From this it could be assumed that vibrational states separated by energy less than 150 cm^{-1} perturb each other and that any combination states which differ in the values of vibrational quantum numbers like $6^1(A')$ and $6^1(A'')$ states had to be considered as interacting. From this point of view the investigated fundamental states $2^1(A')$ and $5^1(A'')$ might be supposed to interact one with another and also with $3^16^1(A')$ state (Table 2). In the same way, we guessed that the third studied fundamental state $5^1(A')$ together with the nearby $3^16^1(A'')$ and $6^2(A')$ states comprise an interacting triad. The next step was to take into account interaction between $6^2(A')$ and $6^1(A')$ $6^1(A'')$ states which should be of the same order and type as for the lower couple of levels, $6^1(A')$ and $6^1(A'')$, mentioned above. After inclusion of the $6^1(A')6^1(A'')$ combination vibrational level into the set of already selected interacting states, the $6^2(A'')$ state should also be added together with other states surrounding it.

More information concerning all the collected states joined in the direct or indirect ways with the investigated fundamental states $2^1(A')$, $5^1(A')$ and $5^1(A'')$ is gathered in Table 2. A hypothesis that all the vibrational states in the described chain were mutually interacting has been confirmed during further analysis of the spectra except for the 3^3 state. In Table 2 the band centers obtained in the present investigation are included as well. To obtain the best

Table 2
Vibrational states of CH_2DI below 1800 cm^{-1}.

Polyads	Vibrational state	This work	Ref. [5]	Estimates from the lower states
	$3^1(A')$	518.8[a]	518	
	$6^1(A')$	709.5[b]	710	
	$6^1(A'')$	862.6[b]	862	
	$3^2(A')$	1031.7		1037
I	**$2^1(A')$**	1173.4	1172	
	$3^1(A')$ $6^1(A')$	1224.0		1228
	$5^1(A'')$	1240.0	1240	
II	$3^1(A')$ $6^1(A'')$	1378.2		1381
	$6^2(A')$	1405.1		1419
	$5^1(A')$	1424.6	1424	
III	$3^3(A')$	–		1556
	$6^1(A')$ $6^1(A'')$	1576.4		1572
IV	$2^1(A')$ $3^1(A')$	1688.4		1692
	$6^2(A'')$	1724.8		1725
	$3^2(A')$ $6^1(A')$	1733.2		1741
	$3^1(A')$ $5^1(A'')$	1756.5		1758

[a] From Ref. [3].
[b] From Ref. [4].

Table 3
Observed bands of CH_2DI.

Band	Band center cm^{-1}	Number of lines	J max	K_a max	RMS deviation $\times 10^{-3}$ cm^{-1}
ν_2	1173.37	5220	87	17	0.220
ν_5 (A′)	1424.58	4768	76	16	0.206
ν_5 (A″)	1240.05	3342	76	15	0.221
$\nu_3 + \nu_6$ (A′)	1223.96	166	78	6	0.259
$\nu_3 + \nu_6$ (A″)	1378.16	92	48	7	0.252
$2\nu_6$ (A′)	1405.07	4698	70	18	0.190
$3^1 6^1(A') \leftarrow 3^1$	705.37	2255	57	11	0.226
$3^1 6^1(A') \leftarrow 6^1(A')$	524.61	594	53	9	0.243
$3^1 5^1(A'') \leftarrow 3^1$	1237.69	705	58	10	0.282
$6^2(A'') \leftarrow 6^1(A'')$	862.21	1259	49	9	0.223
$3^1 2^1 \leftarrow 3^1$	1169.64	1271	63	9	0.273
$3^1 6^1(A'') \leftarrow 6^1(A'')$	709.52	60	47	4	0.292
$3^1 6^1(A'') \leftarrow 3^1$	859.40	2360	63	13	0.207
$6^1(A')6^1(A'') \leftarrow 6^1(A')$	866.87	915	60	7	0.212
$2\nu_3$	1031.70	972	59	10	0.153
$5^1(A') \leftarrow 6^1(A')$	715.06	92	42	7	0.243
$6^2(A') \leftarrow 6^1(A')$	695.55	122	36	7	0.249

results and to precisely account for all the existing resonances between the states we have tried to assign the transitions not only in the fundamental bands, but also to all the combination states involved. Following this procedure, we succeeded in assigning a dozen combination and hot bands badly overlapped by intense fundamental bands. Brief data on all bands used in the fit are given in Table 3 and in graphical form in Fig. 1.

The assignment of transitions in the fundamental and combination bands was carried out by the method of ground state combination differences, while for the hot bands we applied similar method using known rotational levels of the lower vibration states 3^1, 6^1(A″) and 6^1(A′). The key features of the spectra used to carry out initial assignment of almost all bands were the corresponding dense prominent ^PQ or ^RQ branches. The fitting of the spectra was a long and tedious process and was performed as follows. As can be seen from Table 3 and Fig. 1, all 12 excited states can be conditionally separated into four sets (polyads) of relatively close levels. The levels belonging to a polyad were supposed to be in stronger resonances than the states from different polyads. The polyads in Table 3 and Fig. 1 are numbered with Roman numerals and composed of the next vibrational states: 2^1, $3^1 6^1$(A′), 5^1(A″) [I, first polyad], $3^1 6^1$(A″), 6^2(A′), 5^1(A′) [II, second polyad], 6^1(A′)6^1(A″), 3^3 [III, third polyad], $2^1 3^1$, 6^2(A″), $3^2 6^1$(A′) and $3^1 5^1$(A″) [IV, fourth polyad]. At first, transitions of each polyad were fitted separately, leading to preliminary values of interaction parameters. At this stage not all transitions could be fitted to our experimental accuracy. After that, all IR lines were introduced in a combined least squares fit to give an accurate set of band centers, rotational, centrifugal distortion and interaction parameters for 11 vibrational states. At this final stage the parameters of all polyads were refined and in addition the interaction parameters between the states belonging to the different polyads were determined. The parameters obtained together with their associated statistical uncertainties are collected in Tables 4 and 5. It is worth noticing that the dark state 3^3 was not accounted for because the effect from this state was too small to be detected. The $3^2 6^1$(A′) was the only dark state among 11 states. It was found through observed strong shifts in opposite directions of the $K_a = 6$ and 7 levels of the $2^1 3^1$ state caused by nearby $K_a = 5$ and 6 levels of this dark state. Also, it should be noted that we did not insert in the fit the lines deformed or split due to quadrupole moment of iodine nuclei. These were the transitions with low K_a. The number of such lines was relatively small, just several percent. In the fit we used all transitions assigned rather than the energy levels derived from these transitions. The energies of the rotational levels of the 3^1, 6^1(A″) and 6^1(A′) states, which were the lower levels for the hot bands, were fixed to the values obtained in the papers [3,4]. Ground state constants were explored in two ways: fixed to those from Ref. [4] and fitted together with the excited state's parameters. Both approaches led practically to the same results.

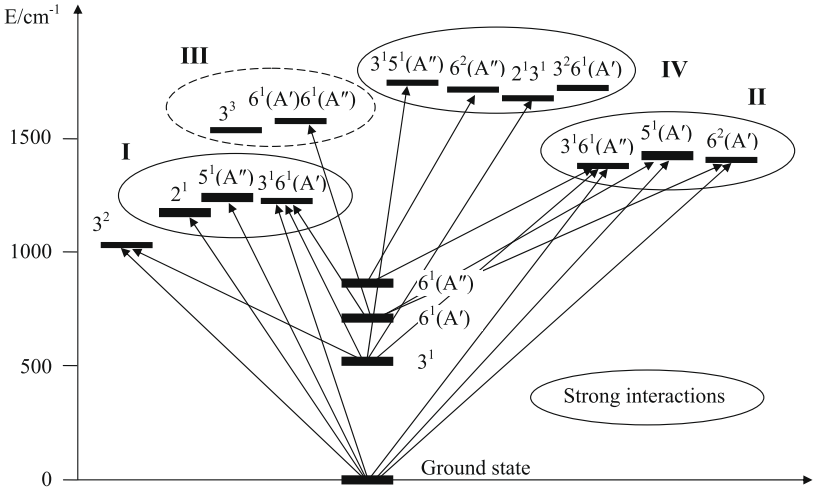

Fig. 1. Assigned and simultaneously fitted bands of CH_2DI.

Table 4
Parameters of the diagonal blocks of the Hamiltonian.

	Ground state	2^1	$3^16^1(A')$	$5^1(A'')$	$3^16^1(A'')$	$6^2(A')$	$5^1(A')$
ν_0		1173.54436(72)	1224.12822(72)	1240.051152(15)	1378.207394(18)	1405.035688(14)	1424.617899(13)
A	3.96627833(45)	3.97684972(44)	3.97924241(86)	3.91028287(78)	3.99026401(89)	3.99151069(50)	3.97970078(54)
B	0.232849805(66)	0.232343140(45)	0.2307193(12)	0.232618380(42)	0.2306231(12)	0.23230879(95)	0.232153651(36)
C	0.229607835(66)	0.228513780(79)	0.227288487(97)	0.229562500(43)	0.227444697(78)	0.229216618(51)	0.228965765(36)
$\Delta_J \times 10^6$	0.174445(23)	0.174588(86)	0.176329(20)	0.175294(14)	0.176605(37)	0.18494(19)	0.16668(19)
$\Delta_{JK} \times 10^6$	2.51274(29)	2.68612(26)	2.4171(17)	2.35196(54)	2.6300(19)	2.0246(58)	2.8588(58)
$\Delta_K \times 10^6$	58.2982(25)	59.3624(40)	58.5835(81)	47.8300(90)	61.233(13)	76.247(76)	53.285(77)
$\delta_J \times 10^9$	2.42011(79)	4.0870(27)	2.056(13)	2.1546(47)	2.713(14)	0.470(21)	0.3406(20)
$\delta_K \times 10^6$	0.4016(28)	0.4016[a]	0.4016[a]	0.4016[a]	0.4016[a]	0.4016[a]	0.4016[a]
$\Phi_J \times 10^{12}$	−0.1162(24)	−0.1037(11)	−0.1692(26)	−0.1545(19)	−0.2010(83)	−0.1225(29)	−0.1311(19)
$\Phi_{JK} \times 10^{12}$	3.059(50)	6.165(44)	5.92(32)	3.12(10)		28.8(12)	−20.3(12)
$\Phi_{KJ} \times 10^9$	0.05521(48)	−0.15611(90)	0.1303(86)	0.0411(25)		−0.611(36)	0.821(36)
$\Phi_K \times 10^9$	3.0621(47)	3.181(11)		−1.759(33)	1.957(60)	11.7145(99)	
	$6^1(A')6^1(A'')$	2^13^1	$6^2(A'')$	$3^26^1(A')$	$3^15^1(A'')$	3^1	3^2
ν_0	1576.451036(22)	1688.398216(22)	1724.789251(69)	1733.1569(53)	1756.445745(37)	518.756481(25)	1031.704701(57)
A	4.0070717(22)	3.9728451(18)	4.0256930(14)	3.97866(43)	3.90726563(16)	3.96231044(99)	3.9583523(38)
B	0.23152685(95)	0.230801836(87)	0.23159112(12)	0.228426(23)	0.23108099(29)	0.231323364(67)	0.22654812(31)
C	0.228230061(70)	0.226955694(94)	0.22834850(12)	0.226716(16)	0.22799993(21)	0.228079626(67)	0.22979110(33)
$\Delta_J \times 10^6$	0.176107(12)	0.176501(20)	0.176301(39)	0.3036(17)	0.176803(74)	0.176160(17)	0.17794(12)
$\Delta_{JK} \times 10^6$	2.5650(14)	2.6917(19)	2.7280(13)	2.51274[a]	2.3547(34)	2.53946(64)	2.5603(29)
$\Delta_K \times 10^6$	59.901(51)	59.100(29)	65.192(20)	103.9(71)	48.499(16)	58.308(11)	58.22(10)
$\delta_J \times 10^9$	2.42011[a]	4.326(20)	2.299(42)	2.42011[a]	2.56(13)	2.5311(48)	2.651(32)
$\delta_K \times 10^6$	0.4016[a]	0.4016[a]	0.4016[a]	0.4016[a]	0.4016[a]	0.445(15)	0.50(11)
$\Phi_J \times 10^{12}$						−0.1164(20)	0.115(24)
$\Phi_{JK} \times 10^{12}$					−17.3(11)	3.48(11)	3.7(11)
$\Phi_{KJ} \times 10^9$		−0.296(32)				0.0453(24)	2.85(72)

Parameters in cm^{-1}. In Tables 4 and 5 the uncertainties in parentheses are one standard deviation in units of the last digit given.
[a] Constrained to the ground state value.

The effective Hamiltonian currently used to analyse the rovibrational spectra of a polyatomic molecule of C_s symmetry in multiple vibrational states is that which was successfully applied, for example, by Baskakov et al. for analysis of the system of seven coupled vibrational states of the formic acid molecule [14]. It presents square operator matrix with a dimension equal to the number of interacting vibrational states, i.e. it was 11 in our case. The diagonal blocks give unperturbed rotational energies of each vibrational state and were chosen to be A reduced Watson's Hamiltonians written in the I^r coordinate representation

$$H = A\hat{J}_a^2 + B\hat{J}_b^2 + C\hat{J}_c^2 - \Delta_J\hat{J}^4 - \Delta_{JK}\hat{J}^2\hat{J}_a^2 - \Delta_K\hat{J}_a^4 + \Phi_J\hat{J}^6 + \Phi_{JK}\hat{J}^4\hat{J}_a^2 + \Phi_{JK}\hat{J}^2\hat{J}_a^4 + \Phi_K\hat{J}_a^6 + [(-\delta_J\hat{J}^2 - \delta_K\hat{J}_a^2 + \varphi_J\hat{J}^4 + \varphi_{JK}\hat{J}^2\hat{J}_a^2 + \varphi_K\hat{J}_a^4, \times (\hat{J}_b^2 - \hat{J}_c^2)]_+$$

$$[\hat{X}, \hat{Y}]_+ = \hat{X}\hat{Y} + \hat{Y}\hat{X}.$$

with

The off-diagonal blocks, which are responsible for Coriolis and Fermi interactions of different types and magnitudes between the levels under consideration, were taken in the form of the series with terms

$$\hat{h}^{\pm}_{n,q,r} = a^{\pm}_{nqr}\hat{J}^{2n}[\hat{J}_a^q,\ (\hat{J}_+^r \pm \hat{J}_-^r)]_+ \quad \text{when } r\neq 0 \text{ and } q\neq 0,$$
$$\hat{h}^{\pm}_{n,q,0} = a^{\pm}_{nq0}\hat{J}^{2n}\hat{J}_a^q \quad \text{when } r = 0,$$
$$\hat{h}^{\pm}_{n,0,r} = a^{\pm}_{n0r}\hat{J}^{2n}(\hat{J}_+^r \pm \hat{J}_-^r) \quad \text{when } r\neq 0 \text{ and } q = 0,$$

where $a^{\pm}_{nqr}$ are the interaction parameters, the a axis is associated with the z axis and $\hat{J}_\pm = \hat{J}_b \pm i\hat{J}_c$ are the angular momentum ladder operators.

4. Analyses and results

The portions of the spectrum of CH_2DI in the region of the $\nu_2(A')$, $\nu_5(A')$ and $\nu_5(A'')$ fundamentals are shown in Figs. 2–4. The $\nu_2(A')$ band has a hybrid a/b appearance, while the $\nu_5(A')$ and $\nu_5(A'')$ bands are of pure b- and c-type, respectively. Since the $5^1(A')$ and $6^2(A')$ states, as was previously noticed by Riter and Eggers [5], are in strong Fermi resonance, the $2\nu_6(A')$ band has almost the same intensity as the $\nu_5(A')$ band. This overtone $2\nu_6(A')$ band consists of mostly b-type transitions and looks like the $\nu_5(A')$ band (Fig. 4).

We will not describe the sequence of actions undertaken for assignment of the transitions in all the bands since it would be too long. We start from a discussion of qualities and features of the parameters obtained. First, it should be noted that they predict all the assigned transitions practically within experimental uncertainties. The set of parameters describes all the observed perturbations and level crossings, some of which are illustrated below. One of the important features of the parameters, which confirm their high quality, is that the quartic centrifugal distortion constants for all the vibrationally excited states do not go far from their respective ground state values. As far as it concerns the coupling parameters, it should be noted that we were not able to determine the constant of Fermi interaction between the $5^1(A')$ and $6^2(A')$ states in spite of the obvious intensity redistribution. Most likely it is because of the strong correlation between the Fermi interaction constant and the corresponding band centers. From this we may conclude that the effective Hamiltonian is obtained in the representation of the strong superposition of the $5^1(A')$ and $6^2(A')$ levels, and the band centers determined are effective rather than deperturbed. It is interesting to compare principal interaction parameters between the couples of states with the similar differences in vibrational quantum numbers. Table 6 presents two main Coriolis coupling constants for the pairs of states derived from the $6^1(A')$, $6^1(A'')$ duet. In the first-order approximation the values of these interaction parameters for different pairs of vibrational states could be readily estimated from the lowest $6^1(A') \leftrightarrow 6^1(A'')$ pair as it is shown in Table 6. On the whole, one can see that all values are of the same order and have expected signs. However, the coupling parameters for the $6^2(A') \leftrightarrow 6^1(A')6^1(A'')$ and

Table 5
Interaction parameters.

Interacting states	Parameter	Value
First polyad		
$2^1 \leftrightarrow 3^1 6^1(A')$	[0, 0, 0, +]	−2.9235(62)
	[0, 0, 1, −]	0.0099681(26)
	[0, 0, 2, +] × 10^4	0.8749(10)
	[1, 0, 1, −] × 10^6	−0.4771(17)
	[2, 0, 1, −] × 10^{10}	0.2439(28)
$2^1 \leftrightarrow 5^1(A'')$	[0, 0, 1, +]	0.0896885(31)
	[0, 0, 2, −] × 10^4	−0.31425(35)
	[1, 0, 1, +] × 10^7	−0.4060(59)
	[0, 0, 3, +] × 10^7	0.1537(29)
	[2, 0, 1, +] × 10^{11}	−0.237(11)
$3^1 6^1(A') \leftrightarrow 5^1(A'')$	[0, 1, 0, +]	−0.015624(23)
	[0, 0, 1, +]	0.024118(12)
	[0, 0, 2, −] × 10^5	−0.185(19)
	[0, 0, 3, +] × 10^6	−0.10468(83)
Second polyad		
$6^2(A') \leftrightarrow 5^1(A')$	[0, 0, 1, −]	0.00548517(99)
	[1, 0, 0, +] × 10^3	−0.687(27)
	[0, 2, 0, +]	0.021106(32)
	[0, 0, 2, +] × 10^4	0.70781(31)
	[1, 0, 1, −] × 10^7	0.2595(42)
	[1, 2, 0, +] × 10^6	−0.260(15)
$6^2(A') \leftrightarrow 3^1 6^1(A'')$	[0, 0, 1, +]	0.0123222(26)
	[0, 0, 2, −] × 10^6	0.1395(17)
	[1, 0, 1, +] × 10^6	−0.7312(28)
	[2, 0, 1, +] × 10^{10}	−0.2659(55)
$5^1(A') \leftrightarrow 3^1 6^1(A'')$	[0, 0, 1, +]	0.0100340(25)
	[1, 0, 1, +] × 10^5	0.10055(26)
	[2, 0, 1, +] × 10^{10}	−0.3446(39)
Fourth polyad		
$2^1 3^1 \leftrightarrow 6^2(A'')$	[0, 0, 1, −]	0.001034(46)
$2^1 3^1 \leftrightarrow 3^2 6^1(A')$	[0, 0, 1, −]	0.0114181(43)
	[0, 0, 2, +] × 10^3	0.11488(24)
$2^1 3^1 \leftrightarrow 3^1 5^1(A'')$	[0, 0, 1, +]	0.0906479(19)
	[1, 0, 1, +] × 10^7	−0.410(18)
$6^2(A'') \leftrightarrow 3^2 6^1(A')$	[0, 0, 0, +]	0.1641(14)
	[0, 0, 1, −] × 10^3	0.726(22)
$6^2(A'') \leftrightarrow 3^1 5^1(A'')$	[0, 0, 1, +]	0.006243(13)
Interactions between polyads		
$3^2 6^1(A') \leftrightarrow 3^1 5^1(A'')$	[0, 0, 1, +]	0.0262534(82)
$3^1 6^1(A') \leftrightarrow 3^1 6^1(A'')$	[0, 0, 1, +]	0.04258(53)
	[0, 0, 2, −] × 10^4	0.3275(85)
$6^2(A') \leftrightarrow 5^1(A'')$	[0, 0, 2, −] × 10^3	0.11760(21)
	[1, 0, 2, −] × 10^8	−0.5658(77)
$6^2(A') \leftrightarrow 6^1(A')6^1(A'')$	[0, 0, 1, +]	−0.03183(63)
	[0, 0, 2, −] × 10^4	−0.2159(54)
$5^1(A') \leftrightarrow 5^1(A'')$	[0, 0, 2, −] × 10^4	0.5304(25)
	[0, 0, 3, +] × 10^7	−0.580(45)
$5^1(A') \leftrightarrow 6^1(A')6^1(A'')$	[0, 0, 2, −] × 10^4	−0.4885(12)
$6^2(A'') \leftrightarrow 6^1(A')6^1(A'')$	[0, 0, 2, −] × 10^4	0.358(12)

For simplicity off-diagonal parameters $a^{\pm}_{nqr}$ denote as [n, q, r, ±].

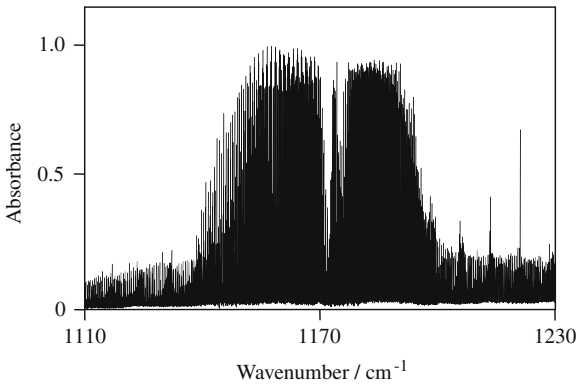

Fig. 2. A survey spectrum of the v_2 band.

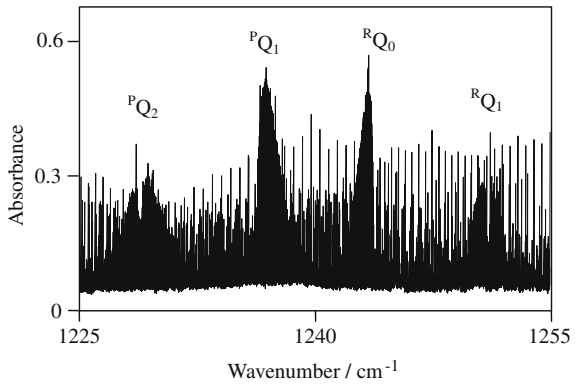

Fig. 3. Portion of the $v_5(A'')$ band.

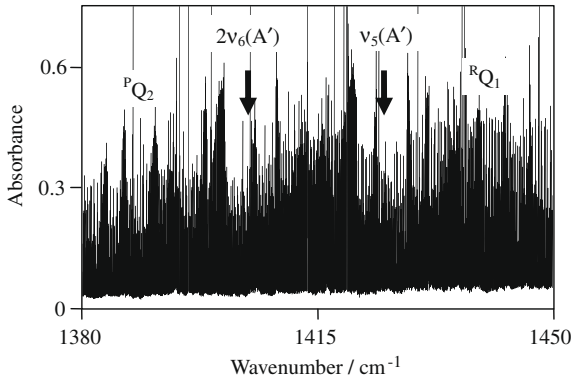

Fig. 4. Region of the central part of the $v_5(A')$ and $2v_6(A')$ bands.

Table 6
Comparison of interaction parameters between couples of the states with the vibrational quantum number differences equal to that for the $6^1(A)$ and $6^1(A'')$ states.

States	[0, 0, 1, +]	[0, 0, 2, −] × 10^4	Estimates[b]
$6^1(A') \leftrightarrow 6^1(A'')$[a]	0.029631(25)	0.32699(38)	A
$3^1 6^1(A') \leftrightarrow 3^1 6^1(A'')$	0.04258(53)	0.3275(85)	A
$6^2(A') \leftrightarrow 6^1(A')6^1(A'')$	−0.03183(63)	−0.2159(54)	$-\sqrt{2}$A
$6^2(A'') \leftrightarrow 6^1(A')6^1(A'')$	Undetermined	0.358(12)	$\sqrt{2}$A

[a] From Ref. [4].
[b] A is a value of interacting parameter for the $6^1(A') \leftrightarrow 6^1(A'')$ states.

$6^2(A'') \leftrightarrow 6^1(A')6^1(A'')$ pairs are less than their estimates and this can be caused by significant interactions of these states with the others.

Most perturbations were observed between the states belonging to the same polyad of the close vibrational levels. They were mainly revealed through intensity anomalies and sometimes as distortions in the spectra due to level crossings. Several manifestations of the interactions between the states are demonstrated below.

As a first example, Figs. 5–8 give comprehensive information on the crossing of the rotational levels of the $3^1 6^1(A'')$ and $6^2(A')$ vibrational states with $K_a = 1$ and 3, respectively, in the region of $J = 36$ and its appearance in the spectrum. Fig. 6 presents the mixing coefficients of these rotational levels. Due to a large mixing between the states for $J = 36$, we observed two transitions to these rotational levels, instead of one as it would be expected in the case of an absence of mutual perturbations.

Figs. 7 and 8 show an appearance of the additional transitions in the $^RQ_0$ and $^RQ_2$ branches of the $2v_6(A')$ and $3^1 6^1(A'') \leftarrow 3^1$ bands,

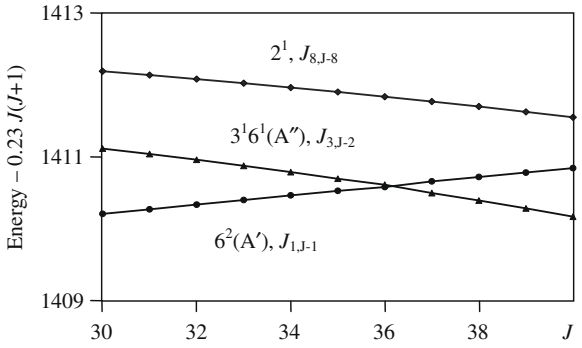

Fig. 5. Crossing of the rotational levels $J_{3,J-2}$ of the $3^16^1(A'')$ state with $J_{1,J-1}$ of the $6^2(A')$ state.

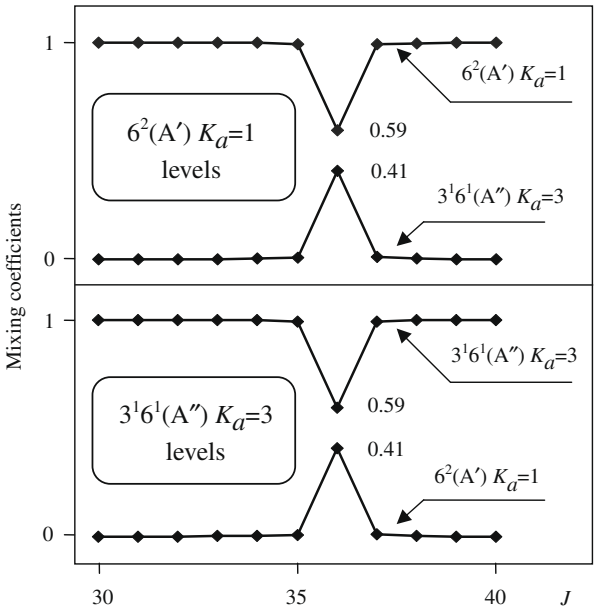

Fig. 6. Mixing of the $6^2(A')$ $K_a = 1$ and $3^16^1(A'')$ $K_a = 3$ level wave functions in the region near crossing.

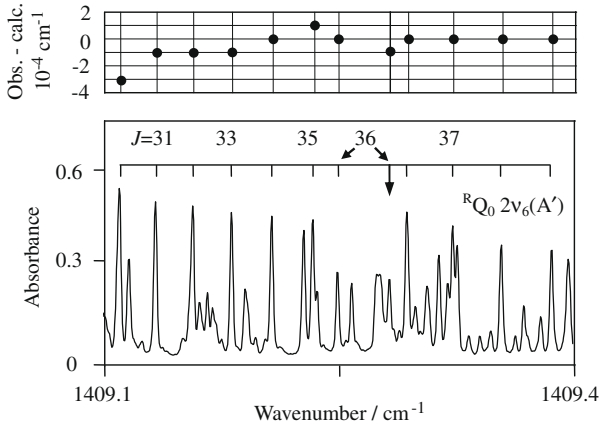

Fig. 7. $^RQ_0$ $2\nu_6(A')$ branch. Appearing of additional line.

which are marked with arrows, and a breaking of the regularity of these branches for $J = 36$. Despite this, the residuals shown in the top of Figs. 7 and 8 obtained with the parameters from Tables 4 and 5 do not exceed experimental uncertainties.

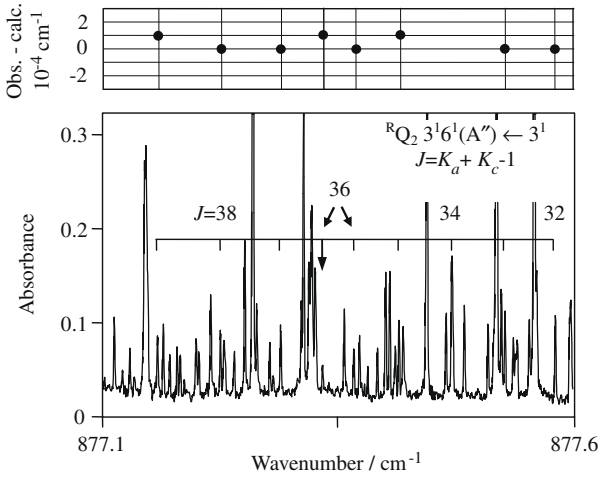

Fig. 8. $^RQ_2$ $3^16^1(A'') \leftarrow 3^1$ hot branch. Appearing of additional line.

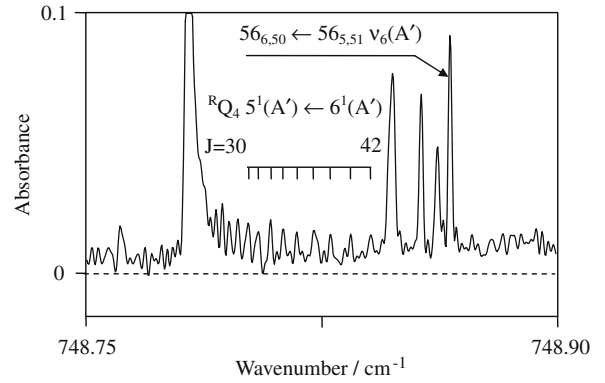

Fig. 9. $^RQ_4$ $5^1(A') \leftarrow 6^1(A')$ hot branch. $56_{6,50} \leftarrow 56_{5,51}$ $\nu_6(A')$ line are marked for comparison of intensities.

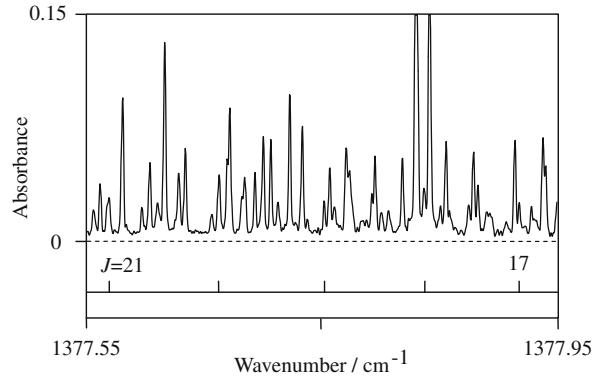

Fig. 10. $^QQ_4$ branch of the $\nu_3 + \nu_6(A'')$ band.

More often, different interactions were observed through abnormal line intensities. An obvious example of this kind of perturbation of the spectrum is an anomalously high intensity of the overtone band $2\nu_6(A')$ mentioned above (Fig. 4). Two other examples of the unexpectedly strong lines recorded in the spectra are given in Figs. 9 and 10.

Fig. 9 presents $^RQ_4$ branch of the $5^1(A') \leftarrow 6^1(A')$ hot band. These lines are seen due to the Fermi interaction of the $5^1(A')$ and $6^2(A')$

vibrational states. Marked lines in Fig. 10 belong to the $^{Q}Q_4$ branch of the $\nu_3 + \nu_6(A'')$ combination band and they became visible due to the interaction of the close rotational levels of the $3^1 6^1(A'')$, $5^1(A')$ and $6^2(A')$ vibrational states with $K_a = 4$, 2 and 3, respectively.

5. Conclusion

This paper presents an extensive study of the FTIR spectra of CH_2DI occupying the vibrationally excited states with energies between 1000 and 1800 cm^{-1}. Only one vibrational state, namely 3^2, out of 12 studied could be analysed satisfactorily as isolated state, and several Fermi- and Coriolis-type interactions, some of which were very weak, had to be taken into account for all other 11 states to reproduce the measured transition wavenumbers within experimental accuracy. In total, 46 coupling terms had to be included in the effective Hamiltonian. The spectroscopic parameters obtained in the present work allow for accurate predictions of the rotational energies in the vibrational states investigated, which could be used for force field calculations of this molecule.

A complete list of all the observations used in the fit, together with the residuals, is given as Supplementary data for this article.

Acknowledgment

Authors thank A.J. Vorobjev for a thorough reading of the text and making the corrections.

Appendix A. Supplementary data

Supplementary data for this article are available on ScienceDirect (www.sciencedirect.com) and as part of the Ohio State University Molecular Spectroscopy Archives (http://library.osu.edu/sites/msa/jmsa_hp.htm).

Supplementary data associated with this article can be found, in the online version, at doi:10.1016/j.jms.2010.02.006.

References

[1] M. Koivusaari, Thesis, University of Oulu, Report Series in Physical Sciences, Report No. 10, 1997.
[2] S. Alanko, Thesis, Acta Univ. Oulu A 321, 1999.
[3] K. Kyllönen, S. Alanko, J. Lohilahti, V.-M. Horneman, Mol. Phys. 102 (2004) 1597–1604.
[4] K. Kyllönen, S. Alanko, O.I. Baskakov, A.-M. Ahonen, V.-M. Horneman, Mol. Phys. 104 (2006) 2663–2669.
[5] J.R. Riter Jr., D.F. Eggers Jr., J. Chem. Phys. 44 (1966) 745–758.
[6] P.P. Das, V.M. Devi, K.N. Rao, J. Mol. Spectrosc. 86 (1981) 202–208.
[7] H.-T. Man, R.J. Butcher, J. Mol. Spectrosc. 119 (1986) 51–55.
[8] P.D. Mallinson, J. Mol. Spectrosc. 55 (1975) 94–107.
[9] F. Willaert, L. Margules, K. Kyllönen, A. Ahonen, H. Sarkkinen, S. Alanko, H. Mäder, J. Demaison, J. Mol. Spectrosc. 248 (2008) 146–152.
[10] T. Ahonen, P. Karhu, V.-M. Horneman, An optimized White-type gas cell for the Bruker IFS 120 high resolution FTIR spectrometer, in: Fifteenth Colloquium on High Resolution molecular spectroscopy, Glasgow, Scotland, 8–13 September, 1997.
[11] http://physics.oulu.fi/irspe/Sivut/cell40-2002.pdf.
[12] V.-M. Horneman, J. Opt. Soc. Am. B 21 (2004) 1050–1064.
[13] V.-M. Horneman, PhD Thesis, Acta Univ. Oulu A 239, 1992, p. 127.
[14] O.I. Baskakov, I.A. Markov, E.A. Alekseev, R.A. Motiyenko, J. Lohilahti, V.-M. Horneman, B.P. Winnewisser, L.R. Medvedev, F.C. De Lucia, J. Mol. Struct. 795 (2006) 54–77.